Topics in Catalysis (2022) 65:1541–1555
https://doi.org/10.1007/s11244-022-01628-z

ORIGINAL PAPER

Transition Metal Hexacyanoferrate(II) Complexes as Catalysts in the Ring-Opening Copolymerization of CO_2 and Propylene Oxide

Guillermo Penche[1] · M. Pilar González-Marcos[1] · Juan R. González-Velasco[1]

Accepted: 6 May 2022 / Published online: 23 May 2022
© The Author(s) 2022

Abstract
The catalytic activity of four transition metal hexacyanoferrate(II) complexes ($Ni_2[Fe(CN)_6]$, $Co_2[Fe(CN)_6]$, $KFe[Fe(CN)_6]$ and $Zn_2[Fe(CN)_6]$) in the ring-opening copolymerization (ROCOP) of CO_2 and propylene oxide (PO) is reported here for the first time and compared with that of other hexacyanometallate compounds. Complexes were prepared by coprecipitation employing *tert*-butanol as complexing agent. X-ray diffraction, Fourier-transform infrared spectroscopy, thermogravimetric analysis, elemental analysis, X-ray fluorescence, scanning electron microscopy, transmission electron microscopy and N_2 physisorption were used to confirm the identity of the obtained materials. Except for $Zn_2[Fe(CN)_6]$, which showed an amorphous nature, the complexes were constituted by aggregates of cubic nanocrystals with intra-crystalline micropores and inter-crystalline mesopores. Gas–solid phase titration with NH_3 revealed the high potential of hexacyanoferrates as Lewis acid catalysts. In the case of $Zn_2[Fe(CN)_6]$, the lack of structural organization led to an extremely high density of acid sites (43 μmol m^{-2}). The resulting copolymers were analyzed via nuclear magnetic resonance spectroscopy and gel permeation chromatography. The studied transition metal hexacyanoferrate(II) catalysts showed mild activity in the target reaction, giving rise to polyethercarbonates with moderate CO_2 content (9.3–18.1 wt%), random configuration (67.0–92.4% of polyethercarbonate linkages), modest molecular weights (M_W, g mol^{-1} = 3400–20,200) and high dispersity ($Đ_M$ = 4.0–5.4). Cyclic propylene carbonate (PC) was also produced (1.4–19.8 wt%). Among all, the $Co_2[Fe(CN)_6]$ complex stands as a potential catalyst for CO_2/PO ROCOP due to its high CO_2 uptake, selectivity and molecular weight of the obtained copolymer.

Keywords New microporous materials · Epoxide · CO_2 utilization · Copolymerization · Biodegradable polymers

1 Introduction

Transition metal cyanometallates are a novel and underexplored class of inorganic coordination polymers (CPs) constituted by two transition metal cations linked through cyanide (CN^-) bridging groups (M-C≡N-T). As in the case of MOFs (Metal–organic frameworks), properties and topology of transition metal cyanometallates are easily tunable through the selection of their constituents: (i) the cyanometallate anion ($[M(CN)_a]^{b-}$) and (ii) the outer transition metal cation (T^{c+}). Because of this, this family of materials covers a wide range of applications including energy storage [1, 2], photochemistry [3, 4], sensors [5], molecular magnets [6], gas-storage [7, 8], molecular sieving [9] or catalysis [10].

Divalent transition metal hexacyanometallates ($T_b[M(CN)_6]_2$) are, by far, the most studied class of cyanometallate compounds. They usually crystallize in an open microporous cubic (Fm-3 m) structure (Fig. 1a) [11, 12]. Their pore size and volume can be tailored, based on inner (M) and outer transition metal cations, which turns these complexes into a moldable class of zeolite-like materials [13]. When the negative charge of the hexacyanometallate ($[M(CN)_6]^{b-}$) block and the positive charge of the divalent transition metal cation (T^{2+}) differ, hexacyanometallates do not meet the oxidation state sum rule. Instead, some molecular $[M(CN)_6]^{b-}$ blocks are randomly vacant in the structure (Fig. 1b). These vacancies provide divalent

✉ M. Pilar González-Marcos
mp.gonzalezmarcos@ehu.eus

Guillermo Penche
guillermo.penche@ehu.eus

Juan R. González-Velasco
juanra.gonzalezvelasco@ehu.eus

[1] Department of Chemical Engineering, Faculty of Science and Technology, University of the Basque Country, UPV/EHU, Barrio Sarriena s/n, 48940 Leioa, Bizkaia, Spain

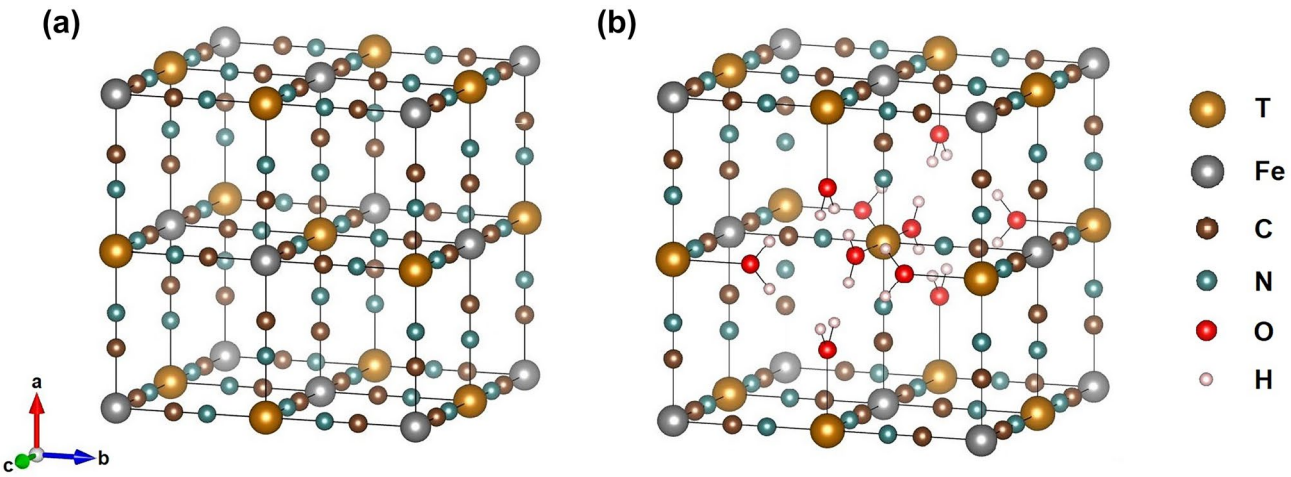

Fig. 1 Crystal network of transition metal hexacyanoferrate(II) complexes **a** without $[Fe(CN)_6]^{3-}$ vacancies and **b** with $[Fe(CN)_6]^{3-}$ vacancies

transition metal hexacyanometallates with open metal sites (OMSs) whose coordination sphere is not fully filled. Their tunable microporosity along with the presence of bulk OMSs make divalent transition metal hexacyanometallates promising solid materials for gas adsorption and catalysis. Of special interest are those complexes derived from the combination of a divalent transition metal cation and a hexacyanometallate(II) anion ($[M(CN)_6]^{4-}$). Charge neutrality is supposed to force vacancies at 50% of the hexacyanometallate(II) blocks, which gives rise to an structure with a high free volume [14].

Catalytic activity of cyanometallates is subject to the presence of the aforementioned OMSs. OMSs are electron-deficient sites and so they act as Lewis acid centers. Cyanometallates have been successfully screened in a huge number of chemical reactions including ring-opening, esterification and transesterification, addition and coupling reactions [10], and they are potential catalysts for any Lewis acid catalyzed reaction. To date, ring-opening polymerization (ROP) of epoxides and ring-opening copolymerization (ROCOP) of epoxides and CO_2 constitute the cornerstone of cyanometallate catalysts.

ROCOP of CO_2 and epoxides represents one of the most successful examples of CO_2 utilization in organic synthesis [15]. It comprises both environmental and economic benefits compared to conventional processes. CO_2 constitutes a very cheap, widely available raw material, which translates into significant cost reduction compared to conventional polymer synthesis processes [16]. The use of CO_2 also helps to valorize a greenhouse gas such as this and to reduce the consumption of oil-derived epoxides, significantly reducing the carbon footprint of the entire process [17]. Moreover, the structure and properties of the resulting aliphatic polycarbonates (APCs) can be easily tuned through the selection of the epoxide monomer, which gives great versatility to this technology. In this sense, propylene oxide (PO) is the most used epoxide because of its price and availability, and the properties of the resulting polymer: polypropylene carbonate (PPC) [18]. PPC has potential applications as films, packaging materials, raw materials for polyurethane industry, biomaterials, adhesives, binders, and so on [18, 19].

Due to the well-known thermodynamic stability and the high kinetic inertness of CO_2 molecules, very active catalysts are required to turn CO_2 into high value-added polycarbonates under mild reaction conditions at appreciable reaction rates. The catalytic system is, in fact, a key parameter when considering the economic viability of the technology. Since Inoue et al. reported the first metal catalyzed copolymerization of CO_2 and PO, several new catalytic systems, both homogeneous and heterogeneous, have been screened in the CO_2/epoxide ROCOP reaction. Homogeneous single-site catalysts allow to obtain perfectly alternating polycarbonates with narrow dispersity indices ($Đ_M$) and high levels of regio- and stereoregularity. Their well-defined structure and soluble nature facilitate in situ mechanistic studies of the copolymerization process, making them especially interesting from an academic point of view. Nevertheless, their impact on the industry is hampered by their limitations in terms of process intensification, expensive reagents, complex synthesis, air sensitivity, and separation troubles. Considering the ligand framework, homogeneous catalysts can be classified as porphyrin, phenoxide, β-diiminate (BDI), and salen systems. Heterogeneous catalysts, on the other hand, present many processing advantages, and so they are preferred in the vast majority of industrial processes. Thus, there are a few examples of already working industrial plants of CO_2-epoxide copolymerization which use heterogeneous catalysts [20–22]. The two main groups of heterogeneous catalysts are zinc carboxylates and cyanometallate complexes. For more detailed information on catalysts for CO_2/

epoxide copolymerization, there are many good reviews to which the reader is referred [18, 23–30].

Cyanometallate complexes constitute one of the most promising classes of heterogeneous catalysts due to their high activity, insensitivity to active hydrogen containing compounds, stability, low price, and ease of synthesis. Several cyanometallate catalysts have been tested in the CO_2/PO ROCOP: $Zn_3[Co(CN)_6]_2$ [31–34], $Zn_3[Fe(CN)_6]_2$ [34–37], $Zn_3[Cr(CN)_6]_2$ [34, 38], $Zn_3[Mn(CN)_6]_2$ [34], $Zn_2[Fe(CN)_6]$ [34], $Zn_2[Mo(CN)_8]$ [34], $Zn[Cd(CN)_4]$ [34], $Zn[Ni(CN)_4]$ [34, 39, 40], $Ni_3[Co(CN)_6]_2$ [41], $Co_3[Co(CN)_6]_2$ [41], $Fe_3[Co(CN)_6]_2$ [41], $Ni_3[Fe(CN)_6]_2$ [41], $Co_3[Fe(CN)_6]_2$ [41], $Fe_4[Fe(CN)_6]_3$ [41], $Co[Ni(CN)_4]$ [40, 42], $Pt[Ni(CN)_4]$ [42] and $Pd[Ni(CN)_4]$ [42]. However, all these catalysts share two common catalytic drawbacks: (i) they tend to incorporate homopolymeric epoxide segments and (ii) they lead to variable amount of cyclic propylene carbonate (PC) as by-product [20, 43] (Fig. 2). These drawbacks have limited the industrial application of cyanometallate catalysts for ROCOP reaction. However, cyanometallate family includes a large number of different complexes, many of which have not been tested yet in the CO_2/epoxide ROCOP and, therefore, their catalytic potential still remains unknown.

In the present work, a series of transition metal hexacyanoferrate(II) compounds was prepared by a coprecipitation reaction between $K_4[Fe(CN)_6]$ and excess of TCl_2 salts (T = Ni^{2+}, Co^{2+}, Fe^{2+} and Zn^{2+}) in the presence of *tert*-butanol (TBA) as complexing agent (CA). The physicochemical properties of the obtained compounds were thoroughly characterized, and their catalytic behavior was tested by ROCOP of CO_2 and PO. Henceforth, transition metal hexacyanoferrate(II) compounds will be referred to as T–Fe.

2 Experimental

2.1 Materials

Potassium hexacyanoferrate(II) ($K_4[Fe(CN)_6]$) was purchased from Sigma Aldrich. Outer transition metal precursor salts ($NiCl_2$, $CoCl_2$, $FeCl_2$ and $ZnCl_2$) were also provided by Sigma Aldrich, with a purity of 98%. TBA (99.5%) and PO (99.5%) were obtained from ACROS Organics. CO_2 was supplied by Air Liquide with a purity of 99.99%. All reagents were used as received.

2.2 Preparation of Transition Metal Hexacyanoferrate(II) Complexes

Transition metal hexacyanoferrate(II) complexes were prepared by a coprecipitation method assisted by a CA following the typical procedure reported in the literature for cyanometallate catalysts [39, 41, 44, 45]. The T/Fe initial preparation ratio was 8, which corresponds to a 300% excess of the stoichiometric requirements. More details are given below.

A 0.16 M aqueous solution of $K_4[Fe(CN)_6]$ (0.006 mol) was added at 5 mL min^{-1} to a 1.6 M aqueous solution of TCl_2 (0.05 mol) containing TBA in a TBA-to-water ratio of 1:3 v/v. The resulting precipitate was aged at 30 °C during 20 min, centrifuged and re-dispersed in a mixture of TBA and water (1:1, v/v). This process was repeated increasing the TBA/water ratio (3:1, v/v). Finally, the solid was suspended in pure TBA, separated by centrifugation and dried at 50 °C under vacuum until constant weight.

2.3 Ring-Opening Copolymerization Procedure

ROCOP reactions were carried out in a 300 mL Autoclave Engineers reactor equipped with a magnetic stirrer, a clamp band heater, and a cooling coil. Prior to the reaction, the desired amount of catalyst was placed in the reactor, which was then closed and purged with N_2 (100 mL min^{-1}) for 30 min. Then, the catalyst was dehydrated in-vacuo for 1 h at the specific catalyst dehydration temperature determined by TGA. Afterwards, the reactor was cooled down to room temperature and PO was fed using a syringe. It was then pressurized with 10 bar of CO_2, to keep PO in the liquid phase, and heated to the desired temperature. Once the reaction temperature (90 °C) was reached, additional CO_2 was added up to 20 bar. Pressure was kept constant along the reaction by feeding fresh CO_2. The reaction was maintained during 24 h. The resulting product was purified by dissolving it in chloroform, then filtered to remove the solid catalyst and dried under vacuum for 24 h at 40 °C.

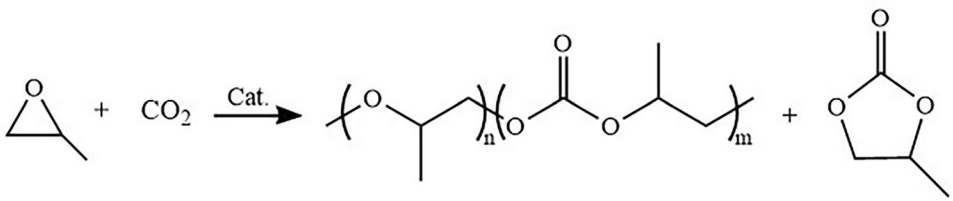

Fig. 2 Scheme of the CO_2/PO ROCOP reaction in the presence of transition metal hexacyanoferrate(II) catalysts

2.4 Characterization

2.4.1 Transition Metal Hexacyanoferrate(II) Complexes Characterization

XRD patterns were obtained in a Philips X'pert PRO using Cu-Kα radiation (λ = 1.541874 Å) with a step size and step time of 0.026° and 598 s, respectively. IR spectra of the studied compounds were collected in a Jasco 4200 FT-IR spectrometer using the KBr pellet method. Inorganic content of the hexacyanoferrates was estimated by X-Ray fluorescence (XRF) analysis (PANalytical/AXIOS wavelength dispersive spectrometer). Elemental Analysis was conducted with a Euro EA Elemental Analyzer (CHNS. EuroVector). Thermogravimetric analysis-mass spectrometry (TGA-MS) was performed in a SETSYS Evolution TGA (Setaram) coupled with an on-line QMG-220 prisma plus compact mass spectrometer (MS, Pfeiffer-Vacuum). TGA-MS measurements were carried out in N_2 flow (50 mL min^{-1}) from 25 up to 950 °C. Scanning electron microscopy (SEM) pictures were obtained from a HITACHI S-4800. Transmission electron microscopy (TEM) micrographs were taken by a JEM-1400 Plus instrument. Textural properties of the complexes were determined by N_2 physisorption at 77 K in a Micromeritics ASAP 2020. Prior to the analysis, samples were pretreated at 150 °C (heating rate of 1 °C min^{-1}) during 10 h in medium-vacuum (around 500 μmHg). OMSs density was determined by gas–solid phase titration with ammonia (NH_3). The samples (about 50 mg) were outgassed at 150 °C for 3 h in a He stream (5 mL min^{-1}) prior to the measurements. Adsorption experiments were conducted in 10% NH_3/He mixture at 100 °C during 1 h. After the adsorption step, samples were evacuated in 50 mL min^{-1} of He gas flow for 2 h to remove weakly absorbed NH_3. Total number of OMSs were determined by assuming a 1:1 stoichiometry for NH_3 adsorption.

2.4.2 Polymer Characterization

Products were characterized by proton nuclear magnetic resonance (^{1}H-NMR) spectroscopy and gel permeation chromatography (GPC). ^{1}H-NMR measurements were carried out on a Bruker AV-500 spectrometer employing $CDCl_3$ as the solvent. GPC analysis was performed on a Waters Breeze HPLC system consisting of a set of Styragel HR-1 and HR-4 columns, binary 515 HPLC pump, Waters 717plus autosampler and a Waters 2414 refractive index detector. System operated at 35 °C employing THF as solvent (flow rate of 1 mL min^{-1}).

3 Results

3.1 Transition Metal Hexacyanoferrate(II) Complexes Characterization

The use of TBA and excess of TCl_2 salts during the synthesis is expected to severely reduce the degree of crystallinity and particle size of the synthesized compounds [46, 47]. This synthesis approach has the aim of increasing the number of defects (bulk and surface defects) in the complexes, which in turn leads to an increase in the density and accessibility of OMSs, and makes transition metal hexacyanoferrate(II) complexes more suitable for catalytic applications. Figure 3a reveals the XRD diffractograms of the prepared compounds.

Ni–Fe, Co–Fe and Fe–Fe samples show similar XRD patterns attributable to a cubic (Fm-3 m) pure phase (ICDD 01-076-5029), which demonstrates that these samples are isostructural, and they have adopted the expected three-dimensional open structure. The Zn–Fe compound shows quite a different pattern, with features of a substantially amorphous substance. This indicates that the crystal structure of the Zn–Fe sample collapsed as a consequence of the synthesis method employed. Zinc-based transition metal cyanometallates usually present deep changes in their degree of crystallinity and crystal symmetry when an excess of the T^{2+} precursor is used together with a CA in the synthesis procedure [46, 48], while other cyanometallates maintain

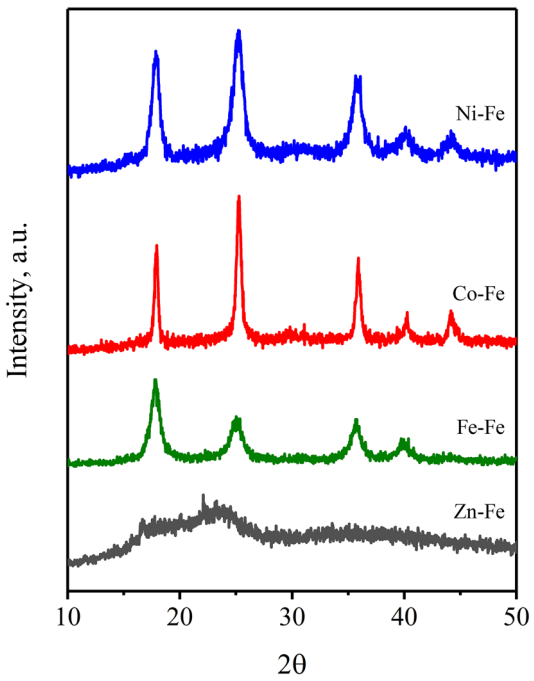

Fig. 3 XRD patterns of the studied transition metal hexacyanoferrate(II) complexes

Table 1 X-ray crystallographic details of the studied transition metal hexacyanoferrates(II)

Sample	Cell edge (Å)	V (Å^3)	Crystallite size (Å)		Strain (ε)
			D–S[a]	W–H[b]	
Ni–Fe	10.04	1011.2	10.5	13.5	0.00153
Co–Fe	10.07	1020.3	23.5	29.5	0.00066
Fe–Fe	10.16	1049.2	8.8	10.1	0.00118

[a]Estimated from Scherrer equation [52]

[b]Determined by Williamson–Hall method [51]

their original cubic structure with minor changes [41]. This phenomenon could be attributed to the tendency of Zn^{2+} to adopt both tetrahedral and octahedral coordination geometries [49], which gives this cation a great versatility when forming different structures. Generally, low crystal symmetry and low crystallinity are associated with high catalytic activity in cyanometallate catalysts [46, 48, 50]. More crystallographic details are attached in Table 1. Due to the inherent disorder coupled to the structure of transition metal hexacyanoferrate(II) complexes, crystallite size was estimated from the Williamson–Hall (W–H) method [51] as well as from the Scherrer equation [52]. The former considers peak broadening due to crystal defects such as vacancies, dislocations, substitutions, etc., so it was considered more accurate in the case of hexacyanoferrate(II) complexes. In fact, the substantially higher crystallite sizes obtained from W–H method evidence the high impact that crystal imperfections have on peak broadening. W–H plots of the studied hexacyanoferrates along with a deeper explanation about the method are attached in Supplementary Material (Fig. S1).

The microstructure of the studied compounds was further analyzed by IR spectroscopy. Figure 4 illustrates the FT-IR spectra of the synthesized samples and $K_4[Fe(CN)_6]$ for comparison. FT-IR spectra of hexacyanoferrates are characterized by three motions related to the octahedral $[Fe(CN)_6]^{4-}$ molecular block: δ(M-CN), ν(M-C) and ν(CN); and two vibration modes from crystal water: ν(OH) and δ(HOH) [53]. The ν(CN) band of cyanometallates helps to confirm the chemical identity of the obtained materials. $K_4[Fe(CN)_6]$ shows this band at 2048 cm^{-1}. Upon coordination to a second transition metal, the frequency of the ν(CN) band shifts to higher frequencies due to σ-donation from nitrogen to the T metal. Herein, the frequency of the ν(CN) band of the complexes is far higher than that of their linear precursor ($K_4[Fe(CN)_6]$), which indicates that the CN^- group has coordinated with a second transition metal via the N atom giving rise to a cyanide-bridged bimetallic structure.

The ν(CN) band frequency is also an indicator of the amount of electron donation from CN^- to metal cations

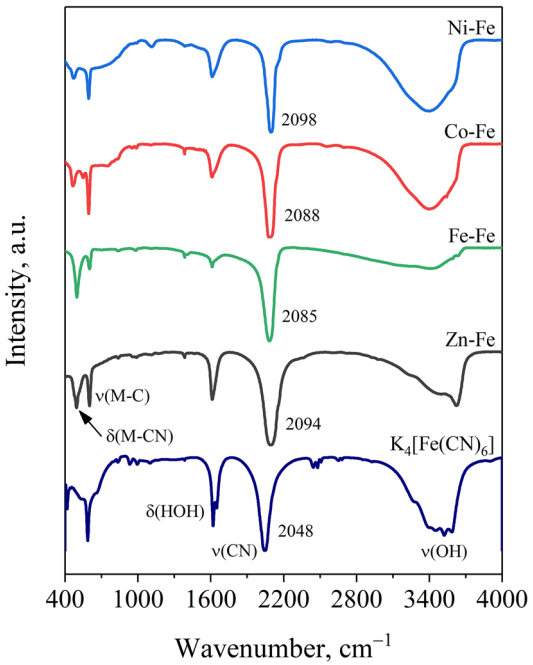

Fig. 4 FT-IR spectra of the studied transition metal hexacyanoferrate(II) complexes

[54, 55]. As a rule of thumb, an increase in IR frequency of the ν(CN) comes as a result of an increase in the amount of electron donation from cyanide bridges to metal ions. Apart from the Zn-Fe complex, which will be discussed later, position of the ν(CN) band increases with electronegativity of the T metal (Ni > Co > Fe) [56]. The Fe–Fe compound shows an intense ν(CN) at 2085 cm^{-1}, which is a frequency significantly higher than that expected for the $Fe^{2+}{}_2[Fe^{2+}(CN)_6]$ complex (ca. 2068 cm^{-1}) [57]. This band would correspond to a Fe^{2+}–C≡N–Fe^{3+} chain, which means that the divalent Fe^{2+} cations have oxidized to Fe^{3+} when exposed to air.

Regarding the Zn–Fe sample, synthesizing zinc(II) hexacyanoferrate(II) from an alkali metal salt (e.g. $K_4[Fe(CN)_6]$ or $Na_4[Fe(CN)_6]$) generally results in a rhombohedral crystal phase in which the Zn^{2+} cation is tetrahedrally coordinated [58]. We synthesized this complex ourselves following the preparation method described above but without using TBA or an excess of $ZnCl_2$. The obtained XRD pattern along with the FT-IR spectrum are attached in Supplementary Material (Fig. S2). The ν(CN) band in this compound is located at frequencies around 2100 cm^{-1}. The blue-shift observed in the Zn–Fe sample prepared with TBA and an excess of $ZnCl_2$ reveals changes in the coordination environment of CN^- groups due to the amorphization of the crystal phase.

CA content is regularly connected with high catalytic activity for cyanometallate complexes in CO_2/epoxide ROCOP reaction [46, 47, 50]. Motions related to the

presence of TBA, δ(OH) around 1380 cm^{-1} and ν(3°–C–O) around 1160 cm^{-1}, could not be identified in any of the samples, which indicates that TBA is not present, or is only residual, in the synthesized compounds.

The bulk chemical composition of the complexes under study was determined by combining XRF, elemental analysis and TGA. Results are summarized in Table 2. Note that the empirical formula could not be estimated for the Fe–Fe complex, since its outer and inner metals are the same. The low T/Fe ratio along with the relatively high K content measured by XRF indicate that Ni–Fe and Co–Fe complexes are a mixture of phases: $T_2[Fe(CN)_6]$ and $K_2T[Fe(CN)_6]$. On the other hand, the high K content observed in the Fe–Fe sample clearly indicates that the actual formula unit of this sample is $KFe^{3+}[Fe^{2+}(CN)_6]$. In alkali-containing hexacyanoferrates(II), K is usually entrapped in the zeolitic cavities of the framework, playing the role of charge compensating ion [59]. The Zn–Fe sample has a considerably lower K content than that expected according to the formula $K_2Zn_3[Fe(CN)_6]_2$, which suggests that this sample is a combination of $K_2Zn_3[Fe(CN)_6]_2$ and $Zn_2[Fe(CN)_6]$ phases. Table S1 shows the expected mass percentage of K for alkali-containing hexacyanoferrates(II) versus the measured percentage obtained from XRF results.

All compounds have a certain Cl content coming from the TCl_2 precursors. The role of Cl in cyanometallate catalysts is still a matter of discussion; however, it has been demonstrated that its presence is necessary to achieve highly active cyanometallate catalysts for both ROP and ROCOP reactions [46, 48].

Organic content of the samples was determined by TGA-MS (Fig. 5). Loss of water occurred at temperatures in the range 25–200 °C. Liberation of TBA could only be identified in the mass spectra of Fe–Fe and Zn–Fe samples (Fig. S3), from a maximum of the ionic current of $C_4H_{10}^+$ (m/z = 41) along with peaks of m/z = 18, which suggests that a process of thermal decomposition with dehydration of TBA occurred. In the absence of catalytic system, dehydration of TBA occurs at temperatures above 400 °C [60]. Thus, considering that the liberation of isobutylene during TGA experiments took place at temperatures as low as 90 °C, we conclude that the OMSs of hexacyanoferrates must play a role in the promotion of TBA dehydration reaction. These results agree with those reported by Chruściel et al. [61] for zinc(II) hexacyanocobaltate(III) ($Zn_3[Co(CN)_6]$) complex. TBA content could not be quantified in the case of the Fe–Fe complex because it overlapped with partial decomposition. This compound showed a weight loss in the range 150–300 °C, which was accompanied by the liberation of mainly CO_2^+ (m/z = 44) but also some CN^+ (m/z = 26). Thus, it was attributed to the decomposition of small particles. Several authors have already reported an early partial decomposition for different hexacyanoferrates [62–64]. Thermal decomposition of the whole samples takes place at temperatures above 350 °C. The extremely low weight of the Zn–Fe residue above 900 °C indicates that part of the metal content is lost during the thermal analysis. Indeed, an XRD (Fig. S4)

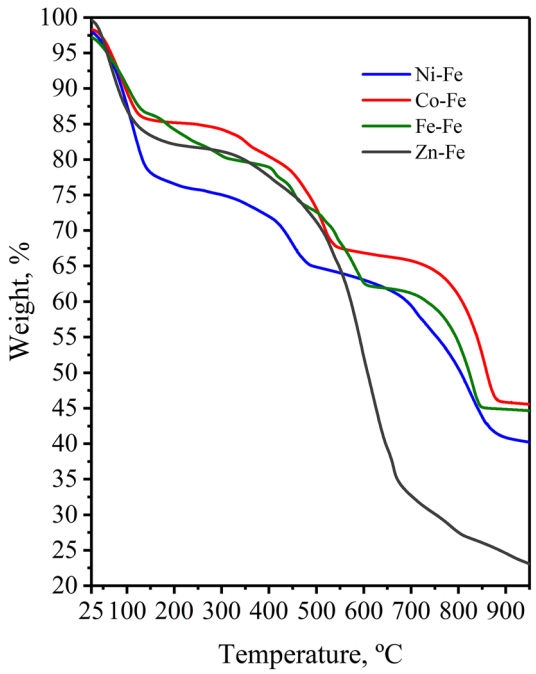

Fig. 5 TG curves of the studied transition metal hexacyanoferrate(II) complexes

Table 2 Elemental analysis of the studied transition metal hexacyanoferrates(II)

Sample	T[a]	M[a]	K[a]	Cl[a]	T/M (at./at.)	C[b]	N[b]	H_2O[c]	TBA[c]	Estimated real catalyst formulation
Ni–Fe	24.4	12.1	7.5	0.7	1.9	14.5	17.9	22.9	–	$K_{0.88}Ni_{1.92}[Fe(CN)_{5.92}]Cl_{0.09}{\cdot}5.89\ H_2O$
Co–Fe	22.1	14.0	11.8	0.9	1.5	16.7	18.7	15.5	–	$K_{1.12}Co_{1.49}[Fe(CN)_{5.32}]Cl_{0.10}{\cdot}3.43\ H_2O$
Fe–Fe	T = M: 38.4		11.6	0.5	–	15.6	18.5	14.7	–	–
Zn–Fe	26.6	13.6	5.4	0.3	1.7	17.6	19.2	16.2	3.1	$K_{0.57}Zn_{1.67}[Fe(CN)_{5.65}]Cl_{0.03}{\cdot}3.69\ H_2O{\cdot}0.17$ TBA

[a]Determined from XRF

[b]Extracted from elemental analysis

[c]Calculated from TGA

plus XRF (Table S2) analysis of the decomposition residue indicated that it contained no zinc.

Transition metal hexacyanoferrate(II) morphology was analyzed by SEM (Fig. 6) and TEM (Fig. 7) microscopy. Samples are composed of shapeless and/or pseudocubic nanoparticles which agglomerate to form particles with diameters in the micrometer range. Fe–Fe sample was obtained with a particularly small particle size, with part of the sample having a colloidal nature. In fact, according to FT-IR and XRF results, this sample is mostly composed by the $KFe^{3+}[Fe^{2+}(CN)_6]$ phase, which is known as "soluble" Prussian blue because it can be easily dispersed in water, due to its colloidal nature, generating a suspension that looks like a solution [65].

TEM images were used to determine primary particle size distribution (PSD) of the studied transition metal hexacyanoferrate(II) complexes. PSD profiles are attached in Supplementary material (Fig. S5). The obtained grain sizes were: 20.2 and 28.0 nm for Ni–Fe and Co–Fe samples, respectively. Grain sizes obtained by TEM analysis were in the range of the crystallite size obtained by peak broadening methods (see Table 1), which is common when the primary particles have a size in the nano-range. Such low particle size values are attributed to the use of TBA during the synthesis. Organic CAs have demonstrated to act as capping agents during cyanometallate crystallite growth, provoking the formation of nanoparticles [47]. The Zn–Fe sample showed a bimodal distribution conformed by small shapeless grains (ca. 24.0 nm) together with large cubic particles (ca. 77 nm). This result indicates that the Zn–Fe sample is a mixture of the expected rhombohedral phase ($K_2Zn_3[Fe(CN)_6]_2$) plus an amorphous phase. These results agree with those observed from XRF. PSD could not be determined for the Fe–Fe sample because of the extremely low size and undefined shape of its particles.

Textural properties of the synthesized transition metal hexacyanoferrate(II) complexes were studied via N_2 adsorption–desorption at 77 K. Figure 8 shows the

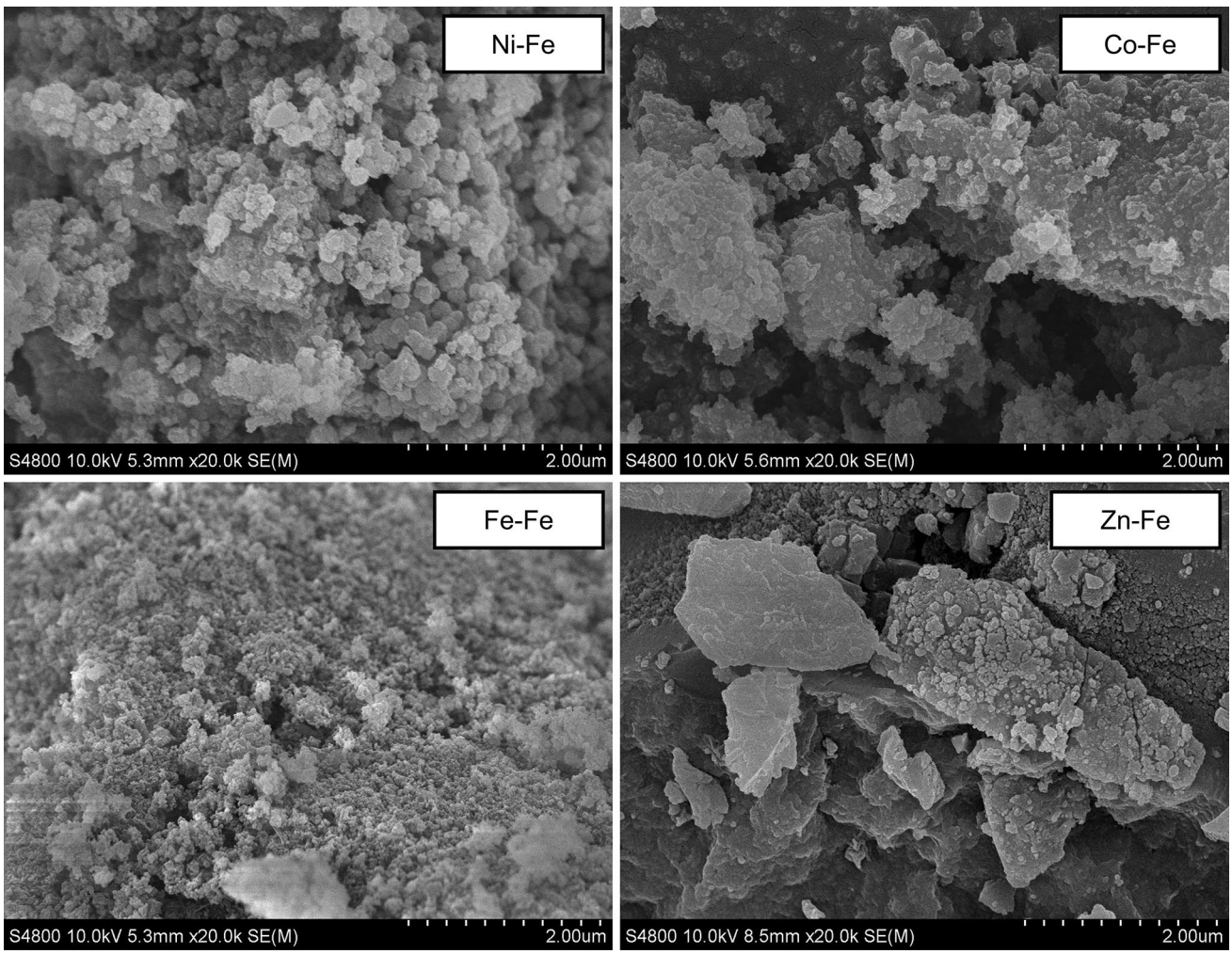

Fig. 6 SEM images of the studied transition metal hexacyanoferrate(II) complexes

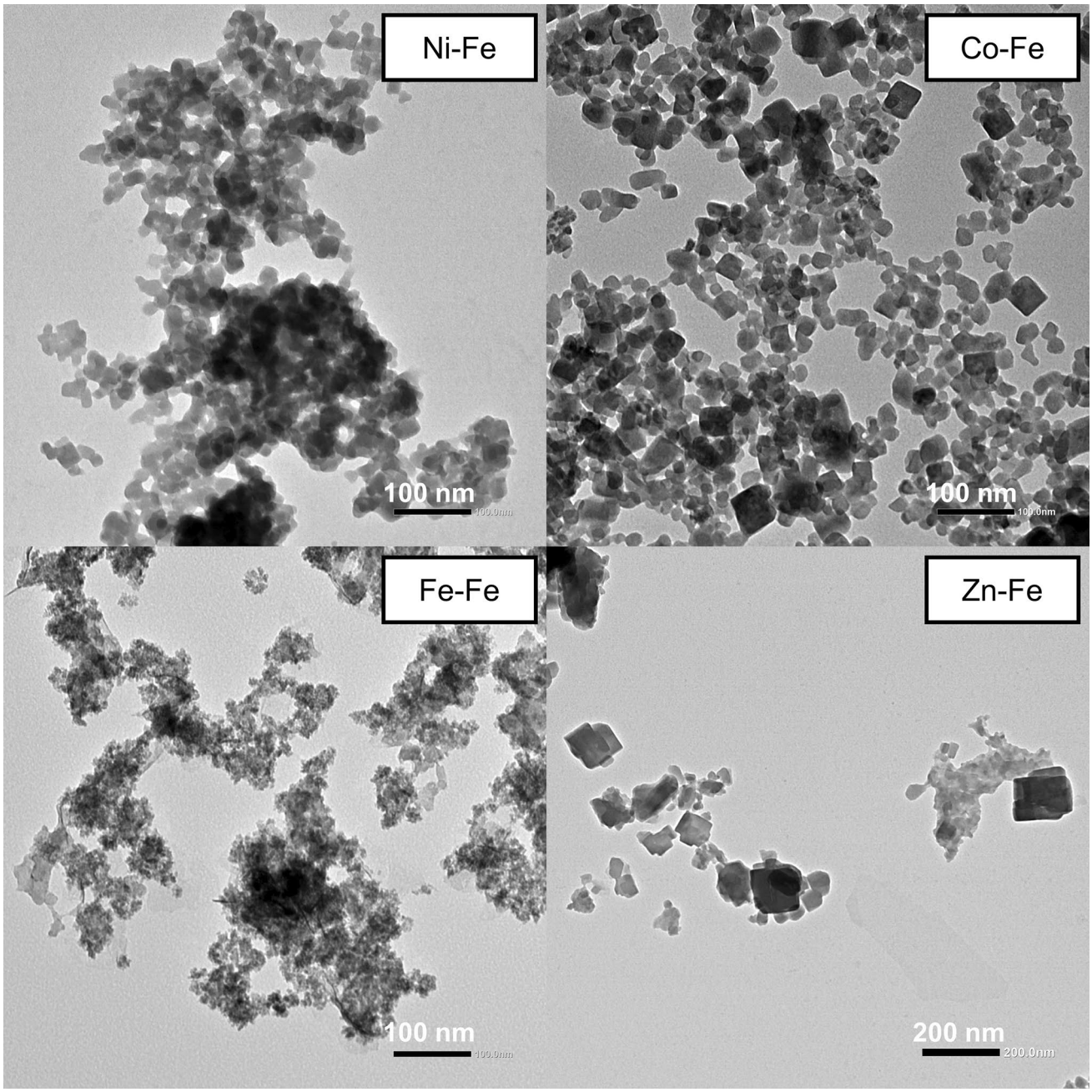

Fig. 7 TEM micrographs of the studied transition metal hexacyanoferrate(II) complexes

adsorption–desorption isotherms of the studied compounds. Table 3 compiles the textural properties of the studied porous hexacyanoferrates. Although transition metal hexacyanoferrates are microporous in nature, hysteresis cycles can be observed due to capillary condensation in the mesoporous region. The nature of such a mesoporous network is attributed to intra-crystalline voids. Indeed, mesoporous average pore diameters (d_{meso}) calculated according to the Barret–Joyner–Halenda (BJH) method [66] are in the range of TEM particle sizes. This hierarchical pore network represents a huge advance from the point of view of catalysis due to the improvement in the mass transfer and diffusional rates that it implies. The microporous framework of the studied compounds resulted practically inaccessible to N_2, as indicated the micropore capacity (V_{micro}) values determined according to different methods (see Table 3). N_2 inaccessibility is attributed to a partial collapse of the porous framework due to heating during pre-treatment [13, 14, 67]. According to Roque et al. [13], this behavior is due to a distortion caused by T metal on the environment of the

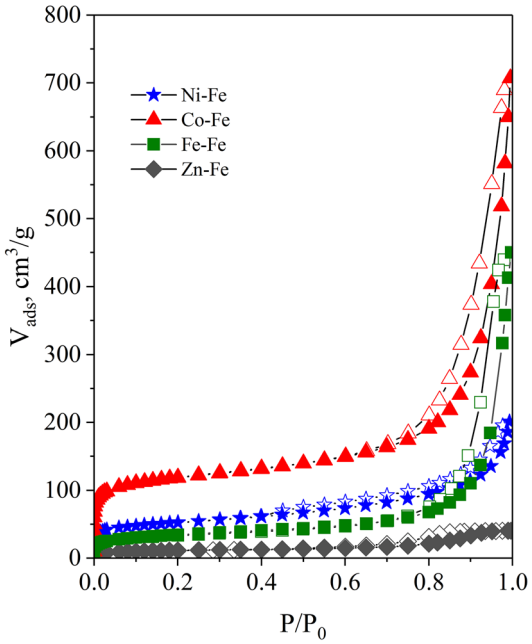

Fig. 8 N_2 adsorption–desorption isotherms of the studied transition metal hexacyanoferrate(II) complexes

Fe atom once it loses its coordinated water molecules. Such distortion results in a reduction of the pore windows cross-section and prevents pore filling with N_2. Moreover, this phenomenon would be modulated by the polarizing power of T^{2+} cation, which would explain why Ni^{2+}–Fe and Fe^{3+}–Fe complexes are especially impenetrable to N_2 molecules [68].

As above mentioned, OMSs are responsible for the catalytic activity in cyanometallate catalysts. Herein, density of OMSs has been measured by gas–solid phase titration, with NH_3 as the probe molecule. Table 4 shows the number of acid sites, expressed in millimole of NH_3 per gram (mmol NH_3 g^{-1}) and millimole of NH_3 per square meter (mmol NH_3 m^{-2}). NH_3 saturation curves are attached in Supplementary material (Fig. S7). In general, the studied hexacyanoferrates show an outstanding surface acidity, which reveals their great potential as heterogeneous Lewis acid catalysts. Particularly remarkable is the extremely high density of OMSs per square meter reached by the Zn–Fe sample because of its amorphous nature.

Table 4 Acid properties of the studied transition metal hexacyanoferrates(II)

Sample	Total acidity (μmol NH_3 g^{-1})	Acid sites density (μmol NH_3 m^{-2})
Ni–Fe	2650	14.2
Co–Fe	990	2.3
Fe–Fe	966	7.9
Zn–Fe	1730	43.3

3.2 Catalytic Activity Tests

Catalytic behavior of the synthesized transition metal hexacyanoferrate(II) complexes was tested in the CO_2/PO ROCOP reaction. Table 5 summarizes the results of the catalytic activity tests. Carbonate unit content (F_{CU}), mass fraction of CO_2 in the polymer (F_{CO2}), weight fraction of PC (W_{PC}) and selectivity of CO_2 (S_{CO2}) and PO (S_{PO}) towards polymers were calculated according to the equations reported elsewhere [41]. The polyethercarbonate-to-polycarbonate linkage ratio (R_{PEC}) was determined following the equation reported by Kember et al. [73].

All studied compounds were active in the target reaction. As far as we are aware, three of these compounds (all except Zn–Fe [34]) are here reported for the first time as active catalytic materials in the ROCOP of CO_2 and PO. The Co–Fe sample showed the highest productivity (TON = 223 mol PO mol Co^{-1}) and catalytic activity (TOF = 9 mol PO mol Co^{-1} h^{-1}). According to our own experience and other works, activity for cyanometallate catalysts in CO_2/epoxide ROCOP reaction is a compromise between many factors,

Table 3 Textural properties of the studied transition metal hexacyanoferrates(II)

Sample	S_{BET}[a] (m^2 g^{-1})	S_{ext}[b] (m^2 g^{-1})	V_t[c] (cm^3 g^{-1})	V_{micro} (cm^3 g^{-1})			d_{meso} (nm[e])
				$V_{m(BET)} = V_{micro} + V_{m(ext)}$[a]	t-plot[b]	D–A[d]	
Ni–Fe	187	112	0.21	0.03	0.03	0.09	13.6
Co–Fe	433	169	0.62	0.09	0.11	0.20	21.0
Fe–Fe	122	48	0.29	0.02	0.02	0.06	27.7
Zn–Fe	40	18	0.06	0.01	0.01	0.02	10.8

[a]Calculated according to the Rouquerol procedure [69]

[b]Determined by t-plot method in the range 6 < t < 9 Å [70]

[c]Measured via the Gurvich-rule at relative pressure (P/P_0) of 0.95 [71]

[d]Extracted from the BJH applied to the adsorption branch [66]. Pore size distribution plots are attached in Supplementary Material (Fig. S6)

[e]Obtained from the Dubinin–Astakhov (D–A) model [72], which has been commonly applied to the study porous cyanometallates [67, 75–77]. More information is attached in Supplementary Material (Table S3)

Table 5 Results of the CO_2/PO ROCOP in the presence of the studied transition metal hexacyanoferrates(II)

Sample	TON[a]	TOF[b]	F_{CU} (mol%)	F_{CO_2} (wt%)	W_{PC} (wt%)	S_{CO_2} (%)	S_{PO} (%)	R_{PEC} (%)	$M_W/M_n/Đ_M$
Ni–Fe	93	4	14.9	10.1	1.4	94.2	99.1	92.4	3600/670/5.4
Co–Fe	223	9	29.3	18.1	5.4	88.2	96.2	67.0	20,200/5000/4.0
Fe–Fe	170	7	13.5	9.3	19.8	46.6	86.6	85.3	14,000/2800/5.1
Zn–Fe	178	7	19.8	13.1	7.5	76.7	95.0	83.8	3400/780/4.4

Reaction conditions: time = 24 h; [Cat] = 2500 ppm; temperature = 90 °C; pressure = 20 bar

[a]TON is expressed in mol PO (mol T)$^{-1}$. Mol of T was determined from the ideal sample formulation: $T_2[Fe(CN)_6]$. In the Fe–Fe sample, ideal formula was substituted by the formula: $KFe[Fe(CN)_6]$

[b]TOF is expressed in mol PO (mol T)$^{-1}$ h^{-1}

including electronegativity of outer and inner transition metal cations, external surface area, density of OMS, content of Cl^-, content of TBA, crystal symmetry and crystallinity [29, 35, 37, 39]. Thus, it was not possible to stablish a direct relationship between the activity and a particular parameter.

The obtained products were characterized via ^{1}H-NMR spectroscopy (Fig. 9). Peak assignment was based on the literature [74]. Signals at 5.0, 4.0–4.3 and 1.34 ppm were assigned to hydrogen atoms of CH, CH_2 and CH_3 groups in carbonate segments, respectively. Their presence evidences the incorporation of CO_2 into the polymer chain. Signals at 3.2–3.8 ppm (CH and CH_2) and 1.14 ppm indicate the presence of ether homopolymeric segments. Production of cyclic PC as by-product is marked by peaks at 4.5, 4.89, 4.04 (the latter two overlapping with peaks of the carbonate segments of the copolymer) and 1.5 ppm.

Since CO_2 incorporation to the polymer was scarce (see Table 5), the obtained polymers must be considered polyethercarbonates (PECs) rather than perfectly-alternating polycarbonates. PC was formed in significant amounts (1.4–19.8 wt%). S_{CO2} was especially low for the Fe–Fe compound. In previous studies, we observed that selectivity of both PO and CO_2 was determined by the electronegativity of the outer transition metal cation [41]. Herein, this trend is still valid for Ni–Fe, Co–Fe and Fe–Fe samples, but not for the Zn–Fe sample. However, the Zn–Fe complex must be remembered to show a structure substantially different from that of the other complexes, in which Zn^{2+} is tetrahedrally coordinated, so its electron density and Lewis strength must be affected.

More information on the microstructure of the copolymers was obtained by analyzing the methyl signal (b) of the carbonate segments (Fig. 9b). Signal in the 1.25–1.32 range (b_1) corresponds to CH_3 in a PEC linkage, whereas signal in the 1.32–1.38 range (b_2) corresponds to CH_3 in a polycarbonate linkage. The ratio between PEC and polycarbonate

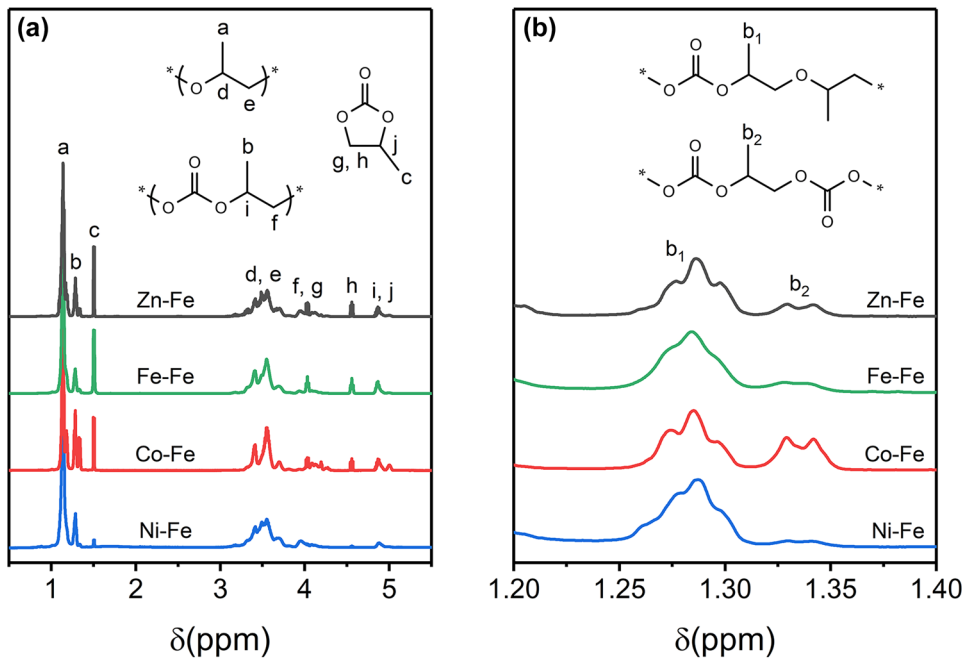

Fig. 9 ^{1}H-NMR spectra of the isolated products **a** between 0.5 and 5.5 ppm and **b** between 1.2 and 1.4 ppm. Supplementary Material provides with detailed ^{1}H-NMR spectra of the products (Figs. S8–S11)

links (R_{PEC}) provides information about the configuration of the polymer chain [73]. A random copolymer would present significant proportion of PEC linkages, while a blocked copolymer would present a low amount of PEC linkages. The synthesized copolymers have very significant proportion of PEC linkages (67–92%), which indicates that they have a random structure.

Polymers showed moderate molecular weights with broad dispersity indices, as expected from heterogeneous catalysts with numerous initiating sites (Fig. 10). M_n values of the PEC chains were shorter than expected according to the equation: $M_n = W_{PEC}/n_{OMS}$, where W_{PEC} and n_{OMS} are the mass of synthesized copolymer and the total moles of catalyst acid sites, respectively. These results are probably due to non-reversible chain transfer reactions with water or other protic impurities during the reaction leading to shorter copolymer chains and higher $Đ_M$ values.

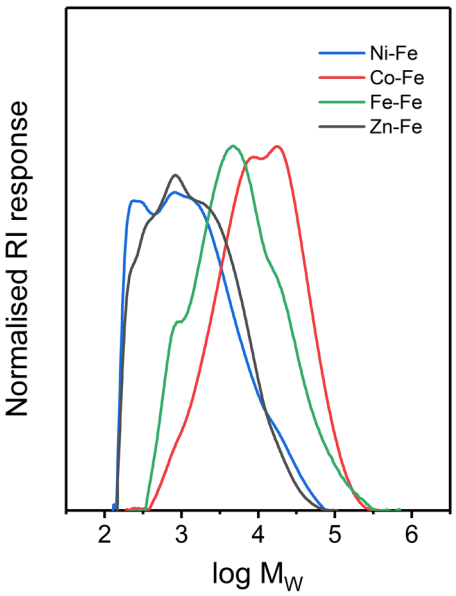

Fig. 10 SEC plots (log Mw) of the PECs produced by the studied transition metal hexacyanoferrate(II) complexes

3.3 Comparison of the Catalytic Behavior of the Synthesized Transition Metal Hexacyanoferrate(II) Compounds with Other Cyanometallate Catalysts

Table 6 compares the catalytic performance of the studied transition metal hexacyanoferrate(II) compounds with that of other hexacyanometallate catalysts reported previously by this group [41]. All catalysts attached in Table 6 have been tested in the same reaction equipment under the same conditions. Additionally, the well-known $Zn_3[Co(CN)_6]_2$-based cyanometallate catalyst (Zn–Co) has also been tested in the CO_2/PO ROCOP reaction in order to compare its catalytic behavior with that of the new complexes herein analyzed. Basic characterization of the Zn–Co catalyst is attached in Supplementary material (Fig. S12).

Table 6 shows that hexacyanometallate complexes lead to random PECs with low CO_2 content and always generate a certain amount of PC. Although the catalytic activities presented by the studied transition metal hexacyanoferrates are in the range of other hexacyanometallate catalysts, they are still far from the industrially employed Zn–Co complex. However, the synthesized complexes outperform this one in terms of CO_2 incorporation and selectivity. In this sense, the Co–Fe complex triples the CO_2 uptake achieved by the Zn–Co catalyst. Moreover, it presents better selectivity

Table 6 Comparison of the performance of the synthesized transition metal hexacyanoferrate(II) complexes with the performance of other hexacyanometallate catalysts

Catalyst ideal formulation	TON[a]	TOF[b]	F_{CU} (mol%)	W_{PC} (wt%)	S_{CO_2} (%)	S_{PO} (%)	R_{PEC} (%)	M_W (g mol^{-1})	$Đ_M$
$Ni_2[Fe(CN)_6]$	93	4	14.9	1.4	94.2	99.1	92.4	3600	5.4
$Co_2[Fe(CN)_6]$	223	9	29.3	5.4	88.2	96.2	67.0	20,200	4.0
$KFe[Fe(CN)_6]$	170	7	13.5	19.8	46.6	86.6	85.3	14,000	5.1
$Zn_2[Fe(CN)_6]$	178	7	19.8	7.5	76.7	95.0	83.8	3400	4.4
$Ni_3[Co(CN)_6]_2$	86	4	22.3	0.4	98.9	99.7	79.5	11,800	10.5
$Co_3[Co(CN)_6]_2$	544	23	20.0	4.2	87.4	97.2	71.9	68,600	4.1
$Fe_3[Co(CN)_6]_2$	428	18	16.3	8.4	73.6	94.5	75.1	85,400	6.3
$Ni_3[Fe(CN)_6]_2$	84	4	24.0	0.6	98.4	99.6	73.9	11,700	15.8
$Co_3[Fe(CN)_6]_2$	296	12	33.5	13.3	75.4	90.2	66.0	50,000	5.9
$Fe_4[Fe(CN)_6]_3$	162	7	17.3	43.1	26.2	67.2	83.3	6000	8.4
$Zn_3[Co(CN)_6]_2$	1279	53	9.7	8.9	61.9	94.4	86.6	8300	2.5

All reactions were run for 24 h at 90 °C and 20 bar of CO_2. Catalysts concentration = 2500 ppm, PO volume = 50 mL

[a]TON is expressed in mol PO (mol T)$^{-1}$

[b]TOF is expressed in mol PO (mol T)$^{-1}$ h $^{-1}$

towards polymers and gives rise to PECs with higher molecular weights.

4 Conclusions

Transition metal hexacyanometallates have gained a great deal of attention over the last few years due to their zeolitic topology and the presence of Open Metal Sites (OMSs) in their structure. These properties make them especially suitable for catalytic purposes. Transition metal hexacyanoferrate(II) complexes stand out due to their theoretical higher free volume and density of OMSs when compared with other hexacyanometallates. Thus, this work presents four transition metal hexacyanoferrate(II) compounds (T–Fe; T = Ni^{2+}, Co^{2+}, Fe^{2+} and Zn^{2+}) synthesized by a TBA-assisted coprecipitation method, whose catalytic activity has been tested in the ROCOP reaction of CO_2 and PO at 90 °C and 20 bar during 24 h.

Ni–Fe, Co–Fe and Fe–Fe compounds crystallized with a cubic (Fm-3 m) unit cell, whereas the Zn–Fe compound showed a lack of crystallinity, presumably as a consequence of the preparation conditions. The bridged bimetallic nature of the obtained materials was confirmed via FT-IR. FT-IR results also revealed that the outer transition metal cation was oxidized in the Fe–Fe sample. The presence of K as charge compensator inside the pores of hexacyanoferrates was identified in all samples by XRF. The high mass percentage of K in the Fe–Fe sample together with the FT-IR results evidence that the true chemical formula of this complex is $KFe[Fe(CN)_6]$, which corresponds with the well-known soluble Prussian blue complex. Cl was also present in the samples, but in extremely low amounts. TBA could only be recognized in Zn–Fe and Fe–Fe samples, an also in extremely low amounts. Both Cl and TBA are supposed to be necessary in order to achieve highly active cyanometallate catalysts for CO_2/PO ROCOP. However, the synthesized complexes showed low tendency to incorporate any of them in their structure. Synthesis conditions led to the formation of hexacyanoferrate(II) nanoparticles which aggregate inducing mesoporosity in the structure. Such mesopore networks are expected to boost the catalytic activity of these compounds, due to the improvement in diffusion and mass transfer issues. The synthesized complexes showed high acidity values when titrated with a basic molecule such as NH_3. The amorphous nature of the Zn–Fe sample gave it an outstanding acid site density of 43.3 μmol m^{-2}.

Transition metal hexacyanoferrate(II) complexes yield random PECs characterized by moderate molecular weights and high dispersity values. PC was formed as a by-product. Except for the Zn–Fe sample, whose structure and local environment of the Zn^{2+} cations were singular, the selectivity of both PO and CO_2 seemed to be controlled by the electronegativity of the outer transition metal cation. Catalytic efficiencies displayed by the studied transition metal hexaycanoferrates(II) are in the range of other hexacyanometallates previously reported, but far lower than that of the $Zn_3[Co(CN)_6]_2$ catalyst. However, considering its high CO_2 uptake, selectivity, and the high molecular weight of the resulting copolymer when compared to the Zn–Co complex, the Co–Fe compound stands as a potential alternative catalyst for ROCOP of CO_2 and PO.

Supplementary Information The online version contains supplementary material available at https://doi.org/10.1007/s11244-022-01628-z.

Acknowledgements The authors thank technical and human support provided by SGIker (UPV/EHU/ERDF, EU).

Author Contributions GP: Validation, Methodology, Investigation, Writing-Original draft preparation. MPG-M: Conceptualization, Methodology, Visualization, Writing-Review & Editing, Supervision. JRG-V: Conceptualization, Supervision, Project administration, Funding acquisition.

Funding Open Access funding provided thanks to the CRUE-CSIC agreement with Springer Nature. This research was funded by the Spanish Ministry of Science and Innovation (Project PID2019-105960RBC21) and the Basque Government (GIC-IT1297-19). One of the authors (G.P.) is the recipient of a PhD research fellowship provided by the Basque Government (PRE_2021_2_0260).

Declarations

Conflict of interest The authors have no relevant financial or non-financial interests to disclose.

Open Access This article is licensed under a Creative Commons Attribution 4.0 International License, which permits use, sharing, adaptation, distribution and reproduction in any medium or format, as long as you give appropriate credit to the original author(s) and the source, provide a link to the Creative Commons licence, and indicate if changes were made. The images or other third party material in this article are included in the article's Creative Commons licence, unless indicated otherwise in a credit line to the material. If material is not included in the article's Creative Commons licence and your intended use is not permitted by statutory regulation or exceeds the permitted use, you will need to obtain permission directly from the copyright holder. To view a copy of this licence, visit http://creativecommons.org/licenses/by/4.0/.

References

1. Lu Y, Wang L, Cheng J, Goodenough JB (2012) Prussian blue: a new framework of electrode materials for sodium batteries. Chem Commun 48:6544–6546. https://doi.org/10.1039/C2CC31777J
2. Okubo M, Asakura D, Mizuno Y, Kim JD, Mizokawa T, Kudo T, Honma I (2010) Switching redox-active sites by valence tautomerism in Prussian blue analogues AxMny[Fe(CN)6]nH_2O (A: K, Rb): robust frameworks for reversible Li storage. J Phys Chem Lett 14:2063–2071. https://doi.org/10.1021/jz100708b

3. Sato O, Iyoda T, Fujishima A, Hashimoto K (1996) Photoinduced magnetization of a cobalt-iron cyanide. Science 272:704–705. https://doi.org/10.1126/science.272.5262.704
4. Pajerowski DM, Andrus MJ, Gardner JE, Knowles ES, Meisel MW, Talham DR (2010) Persistent photoinduced magnetism in heterostructures of Prussian blue analogues. J Am Chem Soc 132:4058–4059. https://doi.org/10.1021/ja100246n
5. Jain AK, Singh RP, Bala C (1982) Solid membranes of copper hexacyanoferrate(III) as thallium(I) sensitive electrode. Anal Lett 15:1557–1563. https://doi.org/10.1080/00032718208064446
6. Bhatt P, Meena SS, Mukadam MD, Yusuf SM (2016) Structural and magnetic properties of Prussian blue analogue molecular magnet $Fe_{15}[Cr(CN)_6]$ mH_2O. AIP Conf Proc 1731:140037. https://doi.org/10.1063/1.4948203
7. Reguera L, Krap CP, Balmaseda J, Reguera E (2008) Hydrogen storage in copper Prussian blue analogues: evidence of H_2 coordination to the cooper atom. J Phys Chem C 112:15893–15899. https://doi.org/10.1021/jp803714j
8. Chapman KW, Southon PD, Weeks CL, Kepert CJ (2005) Reversible hydrogen gas uptake in nanoporous Prussian blue analogues. Chem Commun 26:3322–3324. https://doi.org/10.1039/B502850G
9. Kuyper J, Boxhoorn G (1987) Hexacyanometallate salts used as alkene-oxide polymerization catalysts and molecular sieves. J Catal 105:163–174. https://doi.org/10.1016/0021-9517(87)90016-9
10. Valvekens P, De Vos D (2016) In: Parvulescu VI, Kemnitz E (ed) New materials for catalytic applications, 1st edn. Elsevier, Amsterdam. https://doi.org/10.1016/B978-0-444-63587-7.00001-9
11. Mullica DF, Milligan WO, Beall GW, Reeves WL (1978) Crystal structure of $Zn_3[Co(CN)_6]_2{\cdot}12H_2O$. Acta Crystallogr B 34:3558–3561. https://doi.org/10.1107/S0567740878011589
12. Weiser HB, Milligan WO, Bates JB (1942) X-ray diffraction studies on heavy-metal iron cyanides. J Phys Chem 46:99–111. https://doi.org/10.1021/j150415a013
13. Roque J, Reguera E, Balmaseda J, Rodríguez-Hernández J, Reguera L, del Castillo LF (2007) Porous hexacyanocobaltates(III): role of the metal on the framework properties. Microporous Mesoporous Mater 103:57–71. https://doi.org/10.1016/j.micromeso.2007.01.030
14. Kaye SS, Long JR (2007) The role of vacancies in the hydrogen storage properties of Prussian blue analogues. Catal Today 120:311–316. https://doi.org/10.1016/j.cattod.2006.09.018
15. Liu Q, Wu L, Jackstell R, Beller M (2015) Using carbon dioxide as a building block in organic synthesis. Nat Commun 6:5933. https://doi.org/10.1038/ncomms6933
16. Fernández-Dacosta C, Van der Spek M, Hung CR, Oregionni GD, Skagestad R, Parihar P, Gokak DT, Strømman AH, Ramirez A (2017) Prospective techno-economic and environmental assessment of carbon capture at a refinery and CO_2 utilisation in polyol synthesis. J Carbon dioxide Util 21:405–422. https://doi.org/10.1016/j.jcou.2017.08.005
17. Von der Assen N, Bardow A (2014) Life cycle assessment of polyols for polyurethane production using CO_2 as feedstock: insights from an industrial case study. Green Chem 16:3272–3280. https://doi.org/10.1039/C4GC00513A
18. Cao H, Wang D (2019) In: Zhao Z, Hu R, Qin A, Tang BZ (ed) Synthetic polymer chemistry innovations and outlook. Polymer chemistry series No 32. Royal Society of Chemistry, London. https://doi.org/10.1039/9781788016469-00197
19. Muthuraj R, Mekonnen T (2018) Recent progress in carbon dioxide (CO_2) as feedstock for sustainable materials development: Co-polymers and polymer blends. Polymer 145:348–373. https://doi.org/10.1016/j.polymer.2018.04.078
20. Qin Y, Wang X (2010) Carbon dioxide-based copolymers: environmental benefits of PPC, an industrially viable catalyst. Biotechnol J 5:1164–1180. https://doi.org/10.1002/biot.201000134
21. Ye S, Wang S, Lin L, Xiao M, Meng Y (2019) CO_2 derived biodegradable polycarbonates: synthesis, modification, and applications. Adv Ind Eng Polym Res 2:143–160. https://doi.org/10.1016/j.aiepr.2019.09.004
22. Machat MR, Marbach J, Schumacher H, Raju S, Lansing M, Over LC, Adler L, Langanke J, Wolf A, Leitner W, Gürtler C (2022) Turning CO/CO_2-containing industrial process gas into valuable building blocks for the polyurethane industry. React Chem Eng 7:580–589. https://doi.org/10.1039/D1RE00508A
23. Coates GW, Moore DR (2004) Discrete metal-based catalysts for the copolymerization of CO_2 and epoxides: discovery, reactivity, optimization, and mechanism. Angew Chem Int Ed 43:6618–6639. https://doi.org/10.1002/anie.200460442
24. Lu XB, Darensbourg DJ (2012) Cobalt catalysts for the coupling of CO_2 and epoxides to provide polycarbonates and cyclic carbonates. Chem Soc Rev 41:1462–1484. https://doi.org/10.1039/C1CS15142H
25. Kozak CM, Ambrose K, Anderson TS (2018) Copolymerization of carbon dioxide and epoxides by metal coordination complexes. Coord Chem Rev. https://doi.org/10.1016/j.ccr.2018.08.019
26. Kember MR, Buchard A, Williams CK (2011) Catalysts for CO_2/epoxide copolymerization. Chem Commun 47:141–163. https://doi.org/10.1098/rsta.2015.0085
27. Klaus S, Lehenmeier MW, Anderson CE, Rieger B (2011) Recent advances in CO_2/epoxide copolymerization-new strategies and cooperative mechanism. Coord Chem Rev 255:1460–1479. https://doi.org/10.1016/j.ccr.2010.12.002
28. Liu S, Wang X (2017) Polymers from carbon dioxide: polycarbonates, polyurethanes. Curr Opin Green Sustain Chem 3:61–66. https://doi.org/10.1016/j.cogsc.2016.08.003
29. Lu XB, Ren WM, Wu GP (2012) CO_2 copolymers from epoxides: catalyst activity, product selectivity and stereochemistry control. Acc Chem Res 45:1721–1735. https://doi.org/10.1021/ar300035z
30. Trott G, Saini PK, Williams CK (2016) Catalysts for CO_2/epoxide ring-opening copolymerization. Philos Trans R Soc A 374:2015085. https://doi.org/10.1098/rsta.2015.0085
31. Li Z, Qin Y, Zhao X, Wang F, Zhang S, Wang X (2011) Synthesis and stabilization of high-molecular-weight poly(propylene carbonate) from Zn-Co-based double metal cyanide catalyst. Eur Polym J 47:2152–2157. https://doi.org/10.1016/j.eurpolymj.2011.08.004
32. Chen S, Hua Z, Fang Z, Qi G (2004) Copolymerization of carbon dioxide and propylene oxide with highly effective zinc hexacyanocobaltate(III)-based coordination catalyst. Polymer 45:6519–6524. https://doi.org/10.1016/j.polymer.2004.07.044
33. Gao Y, Qin Y, Zhao X, Wang F, Wang X (2012) Selective synthesis of oligo(carbonate-ether) diols from copolymerization of CO_2 and propylene oxide under zinc-cobalt double metal cyanide complex. J Polym Res 19:9878. https://doi.org/10.1007/s10965-012-9878-5
34. Zhang XH, Chen S, Wu XM, Sun XK, Liu F, Qi GR (2007) Highly active double metal cyanide complexes: effect of central metal and ligand on reaction of epoxide/CO_2. Chin Chem Lett 18:887–890. https://doi.org/10.1016/j.cclet.2007.05.017
35. Guo Z, Lin Q (2014) Coupling reaction of CO_2 and propylene oxide catalyzed by DMC with co-complexing agents incorporated via ball milling. J Mol Catal A 390:63–68. https://doi.org/10.1016/j.molcata.2014.03.006
36. Zhang W, Lin Q, Cheng Y, Lu L, Lin B, Pan L, Xu N (2012) Double metal cyanide complexes synthesized by solvent-free grinding method for copolymerization of CO_2 and propylene oxide. J Appl Polym Sci 123:977–985. https://doi.org/10.1002/app.34544

37. Dai C, Zhu Q, Pang H, Zhu L, Lin Q (2016) Rapid copolymerization of carbon dioxide and propylene oxide catalyzed by double metal cyanide complexes in an ultrasonic field. Mater Lett 180:89–92. https://doi.org/10.1016/j.matlet.2016.05.119
38. Qiang L, Zhifang G, Lisha P, Xue X (2015) Zn-Cr double metal cyanide catalysts synthesized by ball milling for the copolymerization of CO_2/propylene oxide, phthalic anhydride/propylene oxide, and CO_2/propylene oxide/phthalic anhydride. Catal Commun 64:114–118. https://doi.org/10.1016/j.catcom.2015.02.015
39. Chen S, Xiao Z, Ma M (2008) Copolymerization of carbon dioxide and epoxides with a novel effective Zn-Ni double-metal cyanide complex. J Appl Polym Sci 107:3871–3877. https://doi.org/10.1002/app.25064
40. Guo Z, Lin Q, Zhu L, Wang X, Niu Y, Yu C, Fang T (2014) Nanolamellar Zn-Ni/Co-Ni catalysts introduced by ball milling for the copolymerization of CO_2 with propylene oxide. Nanosci Nanotechnol Lett 6:353–356. https://doi.org/10.1166/nnl.2014.1757
41. Penche G, González-Velasco JR, González-Marcos MP (2021) Porous hexacyanometallate(III) complexes as catalysts in the ring-opening copolymerization of CO_2 and propylene oxide. Catalysts 11:1450. https://doi.org/10.3390/catal11121450
42. Robertson NJ, Qin Z, Dallinger GC, Lobkovsky EB, Lee S, Coates GW (2006) Two-dimensional double metal cyanide complexes: highly active catalysts for the homopolymerization of propylene oxide and copolymerization of propylene oxide and carbon dioxide. Dalton Trans. https://doi.org/10.1039/B607963F
43. Luinstra GA (2008) Poly(propylene carbonate), old copolymers of propylene oxide and carbon dioxide with new interests: catalysis and material properties. Polym Rev 48:192–219. https://doi.org/10.1080/15583720701834240
44. Chen S, Zhang P, Chen L (2004) Fe/Zn double metal cyanide (DMC) catalyzed ring-opening polymerization of propylene oxide: part 3. Synthesis of DMC catalysts. Prog Org Coat 50:269–272. https://doi.org/10.1016/j.porgcoat.2004.03.003
45. Sun X, Zhang X, Chen S, Du B, Wang Q, Fan Z, Qi G (2010) One-pot terpolymerization of CO_2, cyclohexene oxide and maleic anhydride using a highly active heterogeneous double metal cyanide complex catalyst. Polymer 51:5719–5725. https://doi.org/10.1016/j.polymer.2010.09.044
46. Zhang X, Hua Z, Chen S, Liu F, Sun X, Qi G (2007) Role of zinc chloride and complexing agents in highly active double metal cyanide catalysts for ring-opening polymerization of propylene oxide. Appl Catal A 325:91–98. https://doi.org/10.1016/j.apcata.2007.03.014
47. Lee IK, Ha JY, Cao C, Park D, Ha C, Kim I (2009) Effect of complexing agents of double metal cyanide catalyst on the copolymerizations of cyclohexene oxide and carbon dioxide. Catal Today 148:389–397. https://doi.org/10.1016/j.cattod.2009.07.073
48. Sebastian J, Srinivas D (2014) Effects of method of preparation on catalytic activity of Co-Zn double-metal cyanide catalysts for copolymerization of CO_2 and epoxide. Appl Catal A 482:300–308. https://doi.org/10.1016/j.apcata.2014.06.007
49. Dudev M, Wang J, Dudev T, Lim C (2006) Factors governing the metal coordination number in metal complexes from Cambridge structural database analyses. J Phys Chem B 110:1889–1895. https://doi.org/10.1021/jp054975n
50. Huang YJ, Qi GR, Chen LS (2003) Effects of morphology and composition on catalytic performance of double metal cyanide complex catalyst. Appl Catal A 240:263–271. https://doi.org/10.1016/S0926-860X(02)00452-0
51. Williamson GK, Hall WH (1953) X-ray line broadening from filed aluminium and wolfram. Acta Metall Mater 1:22–31. https://doi.org/10.1016/0001-6160(53)90006-6
52. Scherrer P (1918) Bestimmung der Grösse und der inneren Struktur von Kolloidteilchen mittels Röntgenstrahlen. Nachr Ges Wiss Gottingen Math Phys Kl 2:98–100. https://doi.org/10.1007/978-3-662-33915-2_7
53. Avila M, Reguera L, Rodríguez-Hernández J, Balmaseda J, Reguera E (2008) Porous framework of $T_2[Fe(CN)_6]xH_2O$ with T= Co, Ni, Cu, Zn and H2 storage. J Solid State Chem 181:2899–2907. https://doi.org/10.1016/j.jssc.2008.07.030
54. Nakamoto K (2009) Infrared and Raman spectra of inorganic and coordination compounds: Part A. Theory and applications in organic chemistry, 6th edn. Wiley, Hoboken. https://doi.org/10.1002/9780470405840
55. Dunbar KR, Heintz RA (1997) In: Karlin KD (ed) Progress in inorganic chemistry, vol 45. Wiley, Hoboken. https://doi.org/10.1002/9780470166468
56. Li K, Xue D (2006) Estimation of electronegativity values of elements in different valence states. J Phys Chem A 110:11332–11337. https://doi.org/10.1021/jp062886k
57. Reguera E, Fernández-Bertrán J, Balmaseda J (1999) The existence of ferrous ferricyanide. Transit Metal Chem 24:648–654. https://doi.org/10.1023/A:1006942415737
58. Renaud A, Cartraud P, Garner E (1979) Proprietes Zeolithiques des ferrocyanures mixtes: isothermes d'adsorption et caracterisation de $K_2Zn_3[Fe(CN)_6]_2$, $9H_2O$. Thermochim Acta 31:243–250. https://doi.org/10.1016/0040-6031(79)85013-3
59. Avila Y, Acevedo-Peña P, Reguera L, Reguera E (2022) Recent progress in transition metal hexacyanometallates: from structure to properties and functionality. Coord Chem Rev 453:214274. https://doi.org/10.1016/j.ccr.2021.214274
60. Barnard JA (1959) The pyrolysis of tert-butanol. Trans Faraday Soc 55:947–951. https://doi.org/10.1039/TF9595500947
61. Chruściel A, Hreczuch W, Czaja K, Sacher-Majewska B (2016) On thermal behaviour of DMC catalysts for ring opening polymerization of epoxides. Thermochim Acta 630:78–89. https://doi.org/10.1016/j.tca.2016.02.009
62. Rodríguez-Hernández J, Reguera E, Lima E, Balmaseda J, Martínez-García R, Yee-Madeira H (2007) An atypical coordination in hexacyanometallates: structure and properties of hexagonal zinc phases. J Phys Chem Solids 68:1630–1642. https://doi.org/10.1016/j.jpcs.2007.03.054
63. Zhang C, Xu Y, Zhou M, Liang L, Dong H, Wu M, Yang Y, Lei Y (2017) Potassium Prussian blue nanoparticles: a low-cost cathode material for potassium-ion batteries. Adv Funct Mater 27:1604307. https://doi.org/10.1002/adfm.201604307
64. Song J, Wang L, Lu Y, Liu J, Guo B, Xiao P, Lee JJ, Yang XQ, Henkelman G, Goodenough JB (2015) Removal of interstitial H_2O in hexacyanometallates for a superior cathode of a sodium-ion battery. J Am Chem Soc 137:2658–2664. https://doi.org/10.1021/ja512383b
65. Davidson D (1937) The formulation of Prussian blue. J Chem Educ 14:277–281. https://doi.org/10.1021/ed014p277
66. Barret EP, Joyner LG, Halenda PP (1951) The determination of pore volume and area distributions in porous substances. I. Computations from nitrogen isotherms. J Am Chem Soc 73:373–380. https://doi.org/10.1021/ja01145a126
67. Balmaseda J, Reguera E, Rodríguez-Hernández J, Reeguera L, Autie M (2006) Behavior of transition metals ferricyanides as microporous materials. Microporous Mesoporous Mater 96:222–236. https://doi.org/10.1016/j.micromeso.2006.06.039
68. Zhang Y (1982) Electronegativity of elements in valence states and their applications. 2. A scale for strengths of Lewis acids. Inorg Chem 21:3889–3893. https://doi.org/10.1021/ic00141a006
69. Rouquerol J, Llewellyn P, Rouquerol F (2007) Is the BET equation applicable to microporous adsorbents? Stud Surf Sci Catal 160:49–56. https://doi.org/10.1016/S0167-2991(07)80008-5
70. Lippens BC, de Boer JH (1965) Studies on pore systems in catalysts V. The t method. J Catal 4:319–323. https://doi.org/10.1016/0021-9517(65)90307-6

71. Rouquerol F, Rouquerol J, Sing K (1999) Adsorption by powders and porous solids. Principles, methodology and applications. Academic Press, London
72. Dubinin MM (1975) In: Cadenheat DA (ed) Progress in surface science and membrane science, 1st edn. Academic Press, New York. https://doi.org/10.1016/B978-0-12-571809-7.50006-1
73. Kember M, Kabir R, Williams CK (2018) Method for preparing polyols. Patent No US20180148539A1. Washington DC: US Patent Office
74. Wang S, Huang Y, Liao B, Lin G, Cong G, Chen L (1997) Structure and properties of poly(propylene carbonate). Int J Polym Anal Chem 3:131–143. https://doi.org/10.1080/10236669708032759
75. Balmaseda J, Reguera E, Gomez A, Roque J, Vazquez C, Autie M (2003) On the microporous nature of transition metal nitroprussides. J Phys Chem B 107:11360–11369. https://doi.org/10.1021/jp027678g
76. Cartraud P, Cointot A, Renaud A (1981) Zeolitic properties of mixed hexacyanoferrate(II): $K_2Zn_3[Fe(CN)_6]_2 \cdot xH_2O$. J Chem Soc Faraday Trans 1(77):1561–1567. https://doi.org/10.1039/F19817701561
77. Balmaseda J, Reguera E, Gómez A, Díaz B, Autie M (2002) Evaluation of cadmium hexacyanoferrate(III) as a microporous material. Microporous Mesoporous Mater 54:282–292. https://doi.org/10.1016/S1387-1811(02)00389-X

Publisher's Note Springer Nature remains neutral with regard to jurisdictional claims in published maps and institutional affiliations.